Nano Energy 124 (2024) 109477

Contents lists available at ScienceDirect

Nano Energy

journal homepage: www.elsevier.com/locate/nanoen

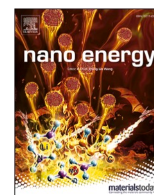

Piezo-optoelectronic coupling in heterojunctions for self-powered and ultrasensitive pressure sensing

Cong Thanh Nguyen [a,*], Emily Lakis [a], Dang D.H. Tran [a], Tuan-Hung Nguyen [a], Jun Sugawara [b], Ivan Gratchev [c], Erik W. Streed [d], Toan Dinh [a,e,f], Nam-Trung Nguyen [a], Van Thanh Dau [c], Dzung Viet Dao [a,c,**]

[a] *Queensland Micro- and Nanotechnology Centre, Griffith University, 170 Kessels Road, Brisbane, Queensland 4111, Australia*
[b] *Department of Transport and Main Roads, Pinkenba, QLD 4008, Australia*
[c] *School of Engineering and Built Environment, Griffith University, Parklands Drive, Gold Coast, Queensland 4222, Australia*
[d] *Institute for Glycomics and Centre for Quantum Dynamics, Griffith University, Parklands Drive, Gold Coast, Queensland 4222, Australia*
[e] *School of Engineering, University of Southern Queensland, 487-535 West Street, Toowoomba, Queensland 4350, Australia*
[f] *Centre for Future Materials, University of Southern Queensland, 487-535 West Street, Toowoomba, Queensland 4350, Australia*

ARTICLE INFO

Keywords:
Semiconductive heterojunction
Silicon carbide
Piezo-optoelectronic coupling
Piezoresistive effect
Optoelectronics
Self-powered pressure sensor

ABSTRACT

It is highly desirable to discover sensing mechanisms for developing self-powered and ultrasensitive pressure sensing. Here, we report that the piezo-optoelectronic coupling in a n^+-3C-SiC/p-Si heterojunction not only enables energy harvesting but also features massive strain sensitivity. To demonstrate the proof of the concept, a pressure sensing device is developed with active and reference electrodes arranged on SiC along strain-sensitive [100] and strain-insensitive [110] orientations, respectively. Under the illumination of 637-nm laser at 2.0 mW, experimental results show the great response of the photogenerated voltage to the change in both static and dynamic pressures. Gauge factor is found to be −670.2 which is much larger than the highest gauge factor of n-type 3C-SiC. The underlying physics behind is the strain modulation on the effective mass and energy level of photogenerated charge carriers. This results in the change in carrier concentration detected by the electrodes along the strain-sensitive and strain-insensitive orientations. These findings could contribute significantly to the development of self-powered mechanical sensors using solid-state electronics.

1. Introduction

Energy-harvesting and self-powered electric and electronic devices are considered as the most effective solutions for the global energy crisis [1]. This concept has been applying to a wide range of sensing devices, such as biosensors [2], wearable sensors [3], implantable sensors [4], and so on. Depending on kinds of energy, respective sensing mechanisms can be applied to convert into electrical power. For instance, mechanical energy from turbine rotations or water tides can be collected by piezoresistive, piezoelectric, electrostatics, or triboelectric effect [5–8]. Thermal energy can be harvested by techniques based on pyroelectric or thermoelectric effect [9,10]. Furthermore, photovoltaic effect-based solar cells are used worldwide for harvesting energy from light which is the most abundant and sustainable energy source [11–13].

Strain-sensitive characteristics in semiconductive materials and structures have been investigated extensively for developing various mechanical sensing devices, such as pressure sensors, accelerometers, and strain gauges [14,15]. Thanks to its high sensitivity, good linearity, simple fabrication, and electronic integration capability, piezoresistive effect is the most dominant mechanism for these applications [16,17]. Therefore, great attention has been paid to enhance the piezoresistive effect after it was discovered by Smith in 1954 [18]. For example, gauge factor was found to be oriented dependent, so the largest gauge factor was obtained along [100] orientation for n-type and [111] orientation for p-type silicon (Si) [19,20]. Material structure and doping concentration are also critical to the strain sensitivity [21,22]. For instance, higher gauge factor of about 20 ∼ 30 at ambient temperature was achieved with single crystalline silicon carbide (SiC) compared to polycrystalline SiC [19,23]. The low density of defects in SiC thin films was experimentally proved to enhance the strain sensitivity by more than

* Corresponding author.
** Corresponding author at: Queensland Micro- and Nanotechnology Centre, Griffith University, 170 Kessels Road, Brisbane, Queensland 4111, Australia.
E-mail addresses: congthanh.nguyen@griffith.edu.au (C.T. Nguyen), d.dao@griffith.edu.au (D.V. Dao).

https://doi.org/10.1016/j.nanoen.2024.109477
Received 2 January 2024; Received in revised form 7 March 2024; Accepted 8 March 2024
Available online 9 March 2024
2211-2855/© 2024 The Authors. Published by Elsevier Ltd. This is an open access article under the CC BY license (http://creativecommons.org/licenses/by/4.0/).

20% [24]. Thanks to recent advances in nanofabrication techniques, the piezoresistance effect in Si nanowires was reported to be about 38 times larger than that in bulk Si [25,26]. This enhancement is substantial however the stability and reliability of the piezoresistive effect and the durability of the sensing devices at such nano scale need further considerations [27].

Interested in self-powered and ultrasensitive sensing mechanisms, this paper investigates for the first time the piezo-optoelectronic coupling in heterojunctions for energy harvesting and pressure sensing. Based on the strain modulation on the mobility and concentration of photogenerated charge carriers, the generated voltage is used to monitor the applied pressure. Regarding self-powered pressure sensors, there are two other sensing principles: piezoelectric effect and triboelectric effect. However, self-powered pressure sensors based on these effects can only detect dynamic pressures [28,29]. Remarkably, the self-powered piezo-optoelectronic pressure sensor developed in this work can measure both static and dynamic pressures. A heterojunction made of highly doped n-type cubic silicon carbide (3C-SiC) on low dop p-type Si (n^+-3C-SiC/p-Si) is used to fabricate sensing devices for demonstration. Reasons for this material selection derive from the great physical, electrical, and chemical properties of 3C-SiC [30,31]. With a wide bandgap (~2.38 eV), 3C-SiC is also electrically stable at elevated temperatures [32]. Combined by wide-bandgap 3C-SiC and narrow-bandgap Si, the heterojunction exhibits great diode properties and is able to harvest energy from a broad range of spectra [33]. The anisotropic strain modulation in 3C-SiC is also advantageous to collect the change in carrier mobility and consequently carrier concentration in different orientations [34]. Finally, cost-effective 3C-SiC/Si wafers have been grown with dimensions up to 300-mm diameter thanks to advanced fabrication techniques [35,36]. Significantly, the photogenerated voltage responses greatly to the change in the applied static and dynamic pressures. Highly sensitive strain sensing with a gauge factor of −670.2 demonstrates the outstanding of the piezo-optoelectronic coupling for self-powered and ultrasensitive pressure sensors.

2. Piezo-optoelectronic pressure sensing mechanism and sensing device

Based on beam bending method, the piezo-optoelectronic coupling in heterojunctions was recently reported [37,38]. This sensing effect is the combination of piezoresistive effect in semiconductors and optoelectronic effect in p-n junctions. Specifically, the coupling is the strain modulation on effective mass and energy band of photogenerated electrons and holes, which results in the change in mobility and concentration of these charge carriers. Considering a pressure sensing diaphragm, Fig. 1**a** illustrates the modulation of photogenerated electrons and holes under the applied bottom-up pressure. An n^+-3C-SiC/p-Si heterojunction is used in this work to demonstrate the proof of the concept. First, a depletion region between the epitaxial n^+-3C-SiC layer and p-Si substrate is formed by the migration of majority charge carriers in opposite directions. The immobile positive and negative ions left behind create the depletion region or space charge region with a built-in electric field toward the p-doped side. Second, if photon energy is larger than the bandgaps of SiC and Si, the illumination will generate a large number of electrons and holes. These photogenerated charge carriers then split to the opposite sides of the space charge region under thermionic emission or drift mechanism. Accordingly, n^+-3C-SiC accumulates photogenerated electrons whereas p-Si amasses photoexcited holes. Third, the applied pressure causes the deformation of the illuminated SiC/Si diaphragm**.** Considering the area within the light penetration depth around the illumination spot, both SiC and Si experience tensile stress. Therefore, the split of valence band and conduction band of photogenerated carriers causes the mass shift or the change in average effective mass, consequently the alteration in mobility and concentration of these charge carriers. For example, the induced tensile strain increases the electron mobility so reducing the electron concentration in 3C-SiC. In summary, the piezo-optoelectronic coupling-based pressure sensing mechanism detects the applied pressure by monitoring the change in the carrier mobility and consequently the carrier concentration.

To demonstrate the piezo-optoelectronic coupling-based pressure sensing mechanism, a sensing device was designed and fabricated using the SiC/Si heterojunction, Fig. 1**b**. A circular diaphragm was formed by etching Si from the back side. Two electrodes were fabricated on top of SiC, an active electrode (E_{act}) along the strain-sensitive orientation [100] and a reference electrode (E_{ref}) on the strain-insensitive direction [110]. Under the applied bottom-up pressure, the stress state on SiC changes continuously from tensile at the center to compressive at the edge. For n^+-3C-SiC, electron mobility increases under tensile stress but decreases under compressive stress. To effectively collect the change in electron concentration, the active electrode was placed in the diaphragm area with no radial stress/strain. In contrast, the reference electrode was designed outside of the diaphragm and along the strain-insensitive orientation [110], which means the carrier concentration is constant in this area. Details of the sensing design can be found in Figure S1. By monitoring the change in the electron concentration between these electrodes, the applied pressure can be determined by the self-powered piezo-optoelectronic pressure sensing mechanism.

Compared to conventional sensors powered by batteries or external energy sources, the piezo-optoelectronic pressure sensor shows its significant advantages. First, the elimination of electrical batteries with

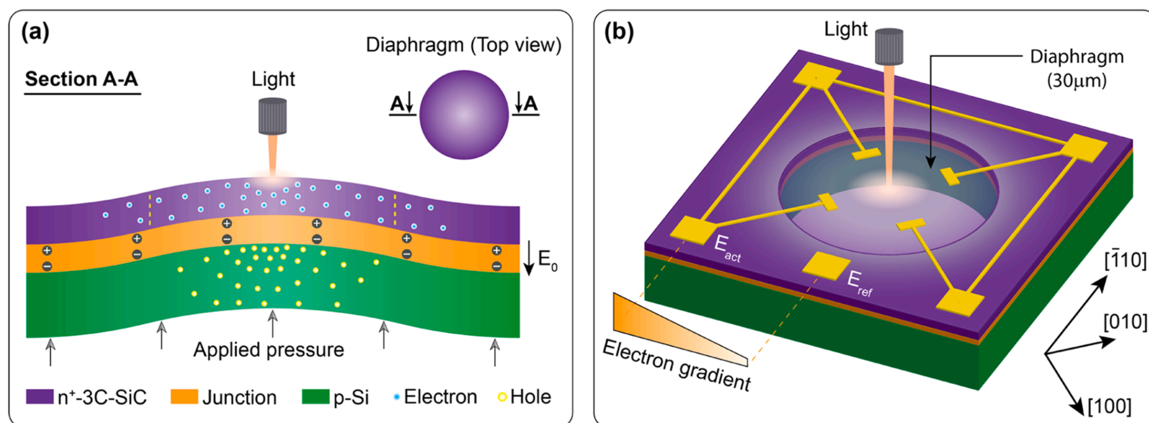

Fig. 1. (a) Pressure sensing mechanism based on the piezo-optoelectronic coupling in heterojunctions. (b) Sensing design with a circular diaphragm made of the 3C-SiC/Si heterojunction. An active electrode (E_{act}) is placed along the strain-sensitive orientation [100] for collecting the change in electron concentration while a reference electrode (E_{ref}) is on the strain-insensitive orientation [110].

limited lifetime enables to reduce manufacturing cost, maintenance cost, and toxic waste. Second, a huge amount of cables can be saved since the developed pressure sensor does not require cables for power connection. With suitable packaging designs, the light-harvesting and self-powered piezo-optoelectronic pressure sensor is great for various applications in smart cities, harsh environments, and so on.

3. Device fabrication and experimental setup

Fabrication process of the SiC/Si pressure sensing chip consists of six main steps, Figure S2. The starting wafer is a commercially available n^+-type 3C-SiC on p-type Si (100) substrate. The 3C-SiC thin film has a thickness of 500 nm ± 10% (Fig. 2**a**) and a doping concentration of about 5×10^{18} cm^{-3}. The Si substrate is 380-µm-thick and doped with boron at a low doping concentration of about 10^{14} cm^{-3}. This epitaxial growth was carried out at 1000 °C with low-pressure chemical vapor deposition using propene and silane precursors [39]. The selected area electron diffraction (SAED) image shows the single crystalline 3C-SiC on Si, Fig. 2**b**. The wafer was first cleaned to remove residual moisture, dust, and fingerprint, step 1. The SiC surface was then sputtered with 500-nm-thick aluminum, step 2. After that, the top aluminum was spin-coated with 1.5-µm-thick AZ1512 photoresist, and then patterned by exposure to ultraviolet light using maskless photolithography, step 3. In step 4, aluminum electrodes were formed by wet etching and then all remaining photoresist was removed. The back side was coated with 10-µm-thick AZ10xT photoresist, following by photolithography (step 5). In the final step, the back side was etched by reactive ion etching (RIE) to create the diaphragm, then residual photoresist was removed. Single sensing chips were separated from the whole wafer by using a diamond pen. Fig. 2**c, d** shows the top side and etching depth of the fabricated sensing chip.

Fig. 2**e** illustrates the experimental setup for characterising the self-powered 3C-SiC/Si pressure sensor under pressure. The sensing chip was attached to a horizontal chip carrier which was assembled to a chamber with pressure precisely manipulated by a pressure controller. After bonding wires and soldering cables, four-point measurement was used to connect the sensing chip to a readout unit (Keithley 2450). A fiber-coupled laser with a wavelength of 637 nm (LP637-SF70, Thorlabs) was mounted on an XYZ translation stage to adjust the laser spot position. Besides, the laser beam on the sensing chip was monitored by a digital microscope (Dino-Lite). The effective beam diameter was tuned to about 100 µm by a beam profiler (BC100006N-VIS, Thorlabs). A power sensor (S130C, Thorlabs) and a power meter (PM100D, Thorlabs) were utilized to adjust the laser power. All the experiments were conducted at ambient temperature in dark conditions.

4. Results and discussion

First, the optoelectronic effect in the 3C-SiC/Si heterojunction was characterized, Fig. 3. Sweeping a bias voltage from −3 to 3 V between the active and reference electrodes, the linear current-voltage curve demonstrates the ohmic contact between SiC and Al, Fig. 3**a**. Significantly, the trivial resistance of metal-semiconductor interface allows to collect almost all photogenerated electrons under the fabricated electrodes. Then, a laser with a wavelength of 637 nm was illuminated on the SiC/Si heterojunction at the diaphragm center. When switching the laser on and off periodically, the repeated change in the photogenerated voltage represents the stable response of the 3C-SiC/Si heterojunction to the light excitation, Fig. 3**b**. While the output voltage is about 0 mV under dark condition, the illumination of 637-nm laser with a power of 2.0 mW results in the output voltage of 7.72 mV. Similarly, Fig. 3**c** shows the great reflection of the photogenerated current between the fabricated electrodes to the repetitive alteration in illumination condition.

The conversion of light illumination to electrical signal is elucidated by the optoelectronic effect or lateral photovoltaic effect in semiconductive heterojunctions. The 637-nm-wavelength laser has a photon energy of about 1.95 eV which is larger than Si bandgap (~1.12 eV). Therefore, electron-hole pairs are released in Si with the photogenerated electron concentration in Si at the excitation point computed as [33,40]:

$$n_{e,Si}(0) = K_1\left(h\nu - E_{g,Si}\right)^{\alpha} \quad (1)$$

where K_1 is the proportional coefficient, α is the exponential coefficient, h is the Planck's constant, ν is the photon frequency, $E_{g,Si}$ is the bandgap

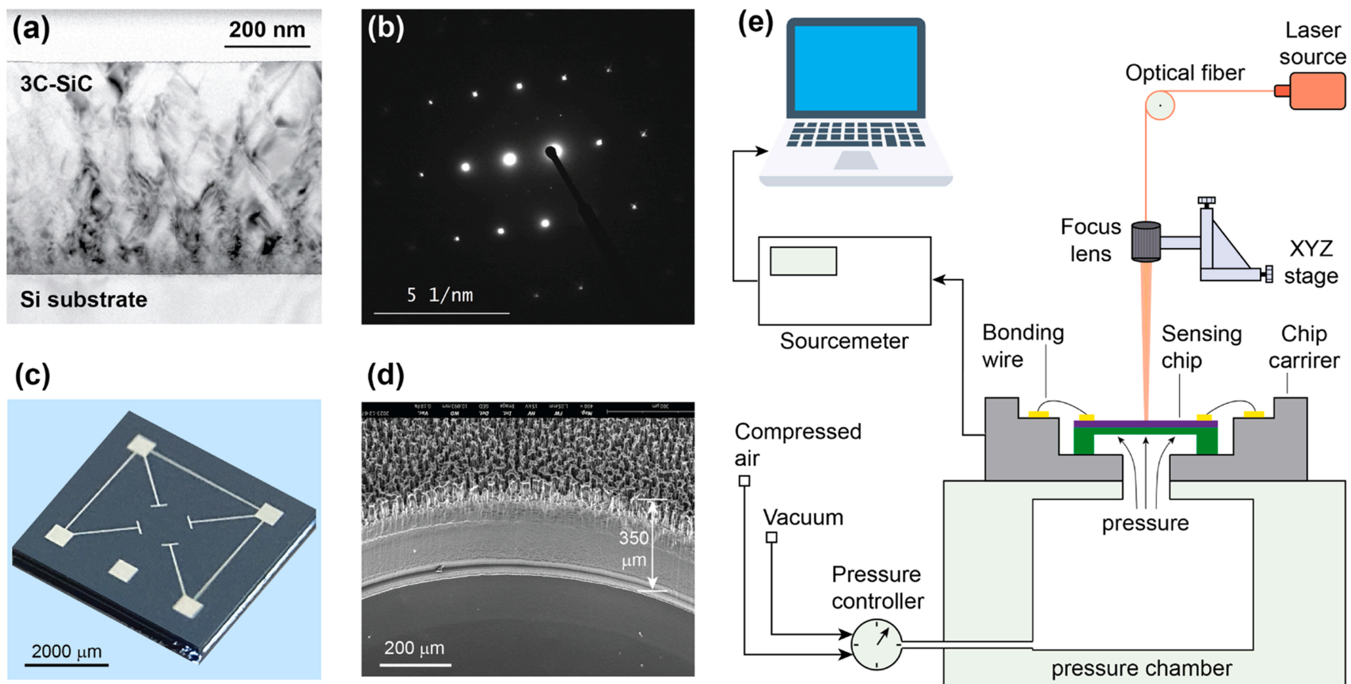

Fig. 2. (a) TEM image of the 3C-SiC/Si heterojunction. (b) SAED image of the 3C-SiC layer. (c) Top-side image of the pressure sensing chip. (d) SEM image shows the etching depth on the back side of the pressure sensing chip. (e) Experimental setup for characterizing the sensing chip under applied pressure.

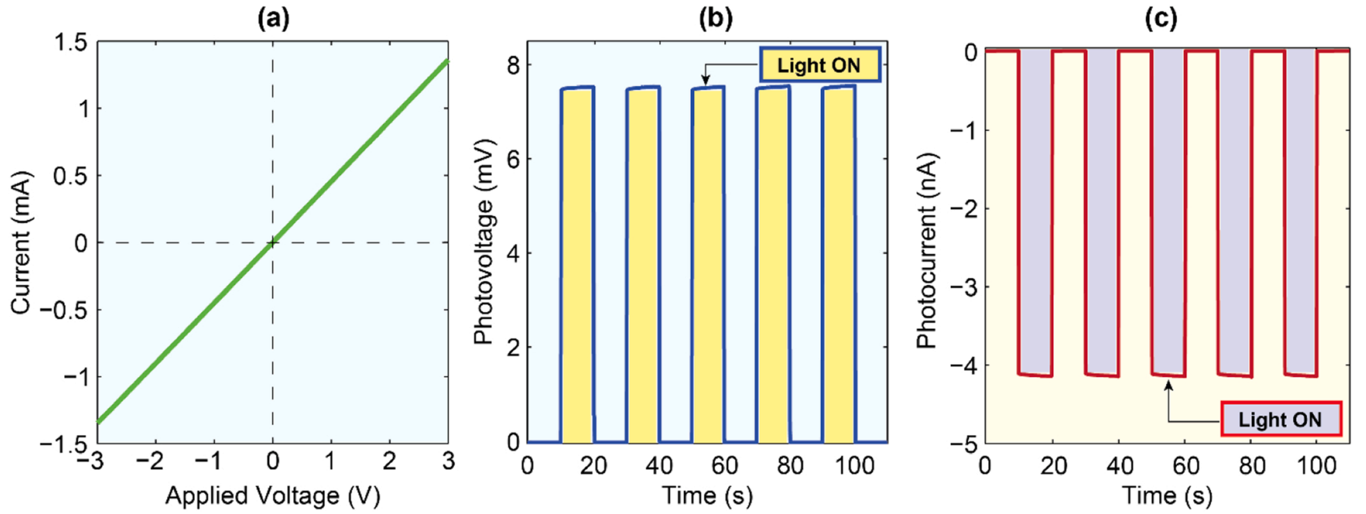

Fig. 3. Characterization of the optoelectronic effect in the 3C-SiC/Si heterojunction. (a) Current-voltage characteristic under dark condition. (b) Photogenerated voltage and (c) Photogenerated current under the excitation of 637-nm wavelength laser with 2.0-mW laser power.

of Si.

The generated electron-hole pairs then split to opposite sides of the depletion region, so holes stay in the Si substrate while electrons pass to the SiC layer. The concentration of migrated electrons at the illumination point in 3C-SiC is calculated as [33,40]:

$$n_{e,SiC}(0) = n_{e,Si}(0)\left[1 - P_1^{\left(\tau P / n_{e,Si}(0)\right)}\right] \tag{2}$$

where P_1 is the possibility of electron recombination, P is the laser power, and τ is the time-related coefficient.

After moving vertically to SiC, the injected electrons diffuse laterally to reduce the concentration. Here, the concentration of nonequilibrium electrons at the distance r from the excitation point is determined by the diffusion equation [41]:

$$D\frac{d^2 n_{e,SiC}(r)}{dr^2} = \frac{n_{e,SiC}(r)}{\tau_{SiC}} \tag{3}$$

where $D = \frac{k_B T}{n\rho q^2}$ is the diffusion coefficient, k_B is the Boltzmann constant, T is the temperature, n is the density of electrons at equilibrium condition, ρ is the SiC resistivity, q is the elementary charge, τ_{SiC} is the lifetime of nonequilibrium electrons in SiC.

The electron concentration at the distance r from the laser position is finally expressed in relation with the concentration at the illumination point as [41]:

$$n_{e,SiC}(r) = n_{e,SiC}(0)\exp\left(-\frac{r}{d}\right) \tag{4}$$

where $d = \sqrt{D\tau_{SiC}}$ is the diffusion length of electrons in SiC.

As the active and reference electrodes are arranged differently with respect to the diaphragm center, meaning their distinct shapes and disparate distances to the illumination spot. As a result, the electron concentration under the active electrode differs from that under the reference electrode, resulting the split of SiC Fermi energy into two quasi-Fermi energy levels at these positions as [42]:

$$E_{F,SiC}(act) = E_{C,SiC} + k_B \ln\frac{n_{e,SiC}(act)}{n_{C,SiC}} \tag{5}$$

$$E_{F,SiC}(ref) = E_{C,SiC} + k_B \ln\frac{n_{e,SiC}(ref)}{n_{C,SiC}} \tag{6}$$

where $n_{e,SiC}(act)$ and $n_{e,SiC}(ref)$ are the electron concentrations under the active and reference electrodes; $E_{C,SiC}$ is the conduction band of SiC; $n_{C,SiC}$ is the intrinsic doping concentration of SiC.

Then, the electric potential measuring between two electrodes under no pressure is computed as:

$$V_{photo,0} \approx \frac{E_{F,SiC}(ref) - E_{F,SiC}(act)}{-q} = \frac{k_B}{q}\ln\frac{n_{e,SiC}(act)}{n_{e,SiC}(ref)} \tag{7}$$

Second, the self-powered piezo-optoelectronic pressure sensing chip was characterized, Fig. 4. The 637-nm laser with a power of 2.0 mW was kept illuminating at the diaphragm center as the previous optoelectronic characterization. The output photogenerated voltage was recorded under different pressure types, including static pressure (Fig. 4**a**), dynamic pressure (Fig. 4**b, c**), and combined static-dynamic pressure (Fig. 4**d, e**). Remarkably, the photovoltage responds greatly to the pressure change from −120 mbar to 1200 mbar. Particularly, the output signal increases stably when the applied pressure is less than the atmospheric pressure, from 7.72 mV at 0 mbar to 7.99 mV at −120 mbar, Fig. 4**a**. Due to the limitation of the used vacuum pump, the pressure of down to −120 mbar is examined. Conversely, the photogenerated voltage reduces under all other positive pressures, Fig. 4**b, c, d, e**. The generated voltage reflects excellently to the cyclic alteration in dynamic since-wave and triangle-wave pressures, Fig. 4**b, c**. The output signal always returns to its initial values when dynamic pressure is removed or reintroduced, demonstrating the great stability and repeatability. It is also noted that the voltage increase under negative pressure (Fig. 4**a**) is comparable to the voltage decrease under positive pressure (Fig. 4**b**). Based on Fig. 4**a, b**, a resolution is determined as 3 mbar which is 0.25% of the full scale. Measurement results are also good when combined static-dynamic pressure in forms of square wave and ramp function are applied, Fig. 4**d, e**. However, the corresponding voltage change is reduced when high pressure is introduced. Consequently, Fig. 4**f** represents the photovoltage change with respect to the applied pressure. Important characteristics of the sensors are summarized in Table 1. Here, the sensitivity is calculated as the ratio between the relative change in output photovoltage and the applied pressure. Considering the relation between applied pressure and output photovoltage, the nonlinearity is computed as the deviation of measurement results from the least-squares regression line. Besides, the returning error is computed approximately as the error in output photovoltage at zero pressure in comparison with the full-scale output (FSO). To evaluate the strain sensitivity, gauge factor (*GF*) is computed as the fractional change in the photovoltage divided by the applied pressure:

$$GF = \frac{\Delta V_{photo}}{V_{photo,0}} \times \frac{1}{\varepsilon_r} = \frac{V_{photo,p} - V_{photo,0}}{V_{photo,0}} \times \frac{1}{\varepsilon_r} \tag{8}$$

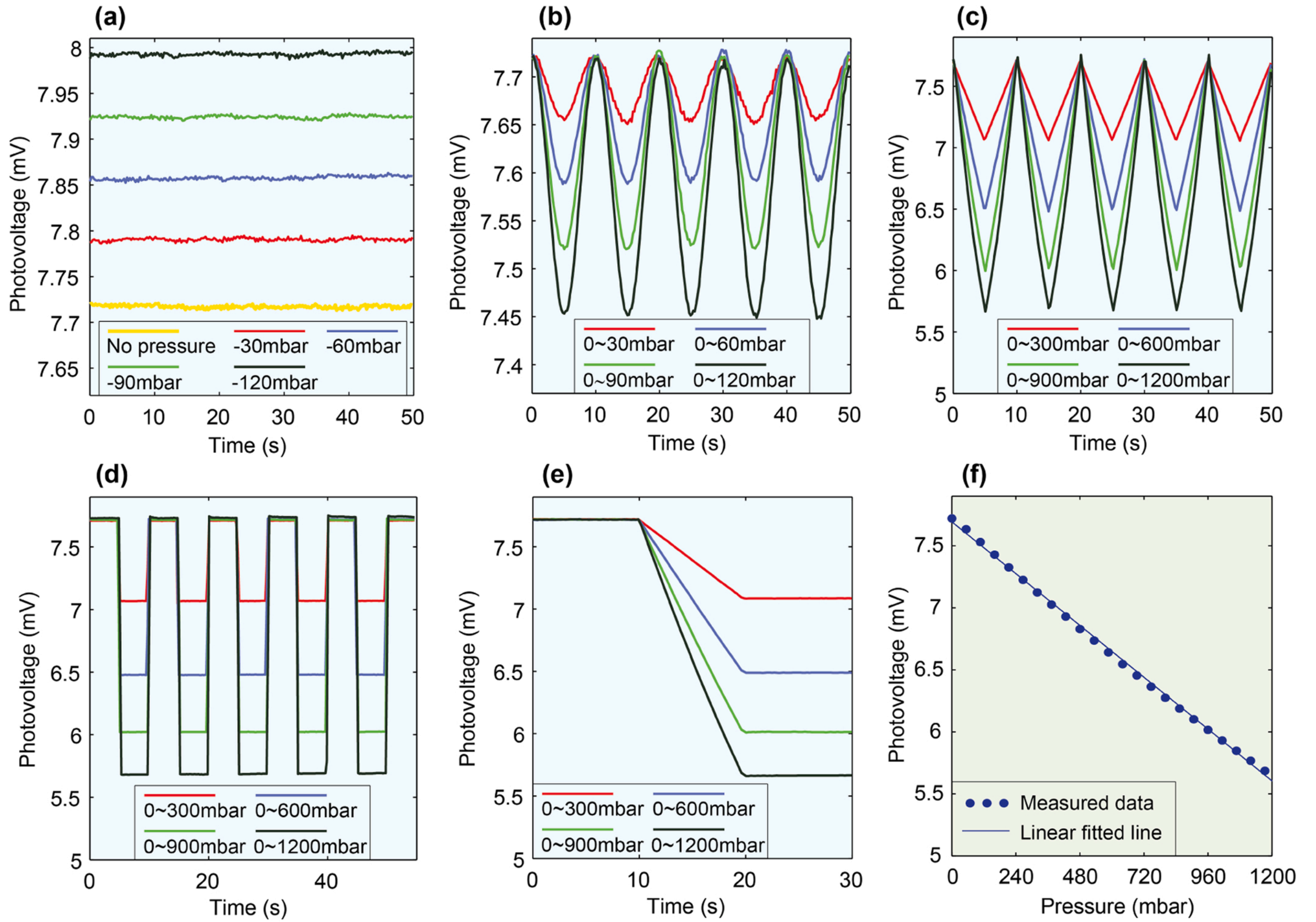

Fig. 4. Characterization of the piezo-optoelectronic pressure sensor under the illumination of 637-nm laser at 2.0-mW power. (a) Under constant pressure. (b) Under since-wave pressure. (c) Under triangle-wave pressure. (d) Under square-wave pressure. (e) Under ramp pressure. (e) Relation between the photogenerated voltage and applied pressure.

Table 1
Characteristics of the self-powered piezo-optoelectronic pressure sensor.

Parameter	Value
Diaphragm diameter	2000 μm
Diaphragm thickness	30 μm
Pressure full-scale (FS)	1200 mbar
Supply laser power	2.0 mW
Offset voltage	7.72 mV
Full-scale output (FSO)	2.05 mV
Sensitivity	1.71 mV/bar
Resolution	0.25% FS
Maximum nonlinearity	4.5% FSO
Returning error	0.56% FSO

where ΔV_{photo} is the change in the photovoltage, $V_{photo,p}$ is the photovoltage under applied pressure, and ε_r is the maximum strain on the diaphragm.

The radial strain appearing in the diaphragm center is computed for all cases of applied pressure, ranging from −120 mbar to 1200 mbar. For example, the radial strain in the diaphragm center is 1.22×10^{-4} under the introduction of 300-mbar pressure from the back side, Figure S3. The gauge factor is finally found to be −670.2 which is much larger than the highest *GF* of 3C-SiC (−31.8 for n-type 3C-SiC, 30.3 for p-type 3C-SiC) [19,20].

Third, the piezo-optoelectronic pressure sensing chip was tested at different laser powers from 0.1 mW to 2.0 mW, Fig. 5. Under no pressure, the photogenerated voltage increases significantly from 0.81 mV at 0.1 mW to 6.45 mV at 1.0 mW, Fig. 5**a**. The photovoltage tends to be saturated when increasing the laser power further. Fig. 5**b** presents the photovoltage change when the applied pressure is ramped up from 0 to 300 mbar. The photogenerated voltage under no pressure is considered as a reference for calculating the photovoltage change. The change can be observed clearly when the laser power is larger than 1.0 mW. Besides, unwanted noise is small at 2.0 mW as the laser condition at this power is more stable. Finally, the relation between the photovoltage change and applied pressure is shown in Fig. 5**c**. The relation is nonlinear at high pressure which is common with other pressure sensors. The obtained GFs are −323.8, −512.1, and −578.5 at 0.1, 1.0, and 1.5 mW, respectively.

Fig. 6 explains the obtained experimental results using the physical mechanism of the self-powered piezo-optoelectronic pressure sensor. Applying pressure from the back side induces radial and tangential tensile strains in SiC around the illumination spot, Fig. 6**d** and Figure S3. The effect of the tangential stress on the generated photovoltage can be ignored since the active electrode is arranged tangentially on the diaphragm. Moreover, it is noted that the photogenerated electrons at the illumination spot or diaphragm center diffuse toward the active electrode along the orientation [100]. Therefore, the induced radial stress along this direction is critical to the electron concentration under the active electrode. Fig. 6**a** illustrates the split of conduction bands and consequently the repopulation of photogenerated electrons along the

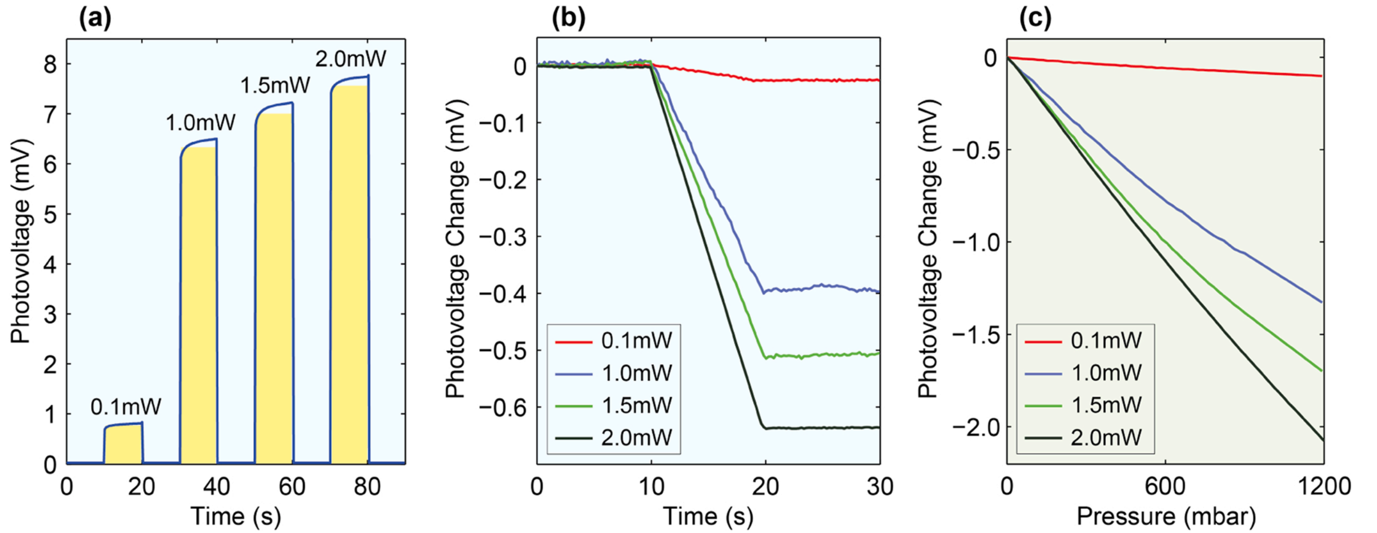

Fig. 5. Characterization of the piezo-optoelectronic pressure sensor under the illumination of 637-nm laser at different powers. (a) Photogenerated voltage under no pressure. (b) Photovoltage change when pressure is ramped up from 0 to 300 mbar. (c) Relation between the photovoltage change and applied pressure.

interested orientation [100] and no-strain direction [001]. The upper right inset represents six equivalent ellipsoid energy valleys in the conduction bands of n-3C-SiC under no pressure. These energy ellipses coincide with six corresponding <100> directions in k-space. The effective mass of electrons in a single energy ellipse is anisotropic or depends on orientations. The smaller energy curvature of these ellipses means the larger effective mass [34]. In other words, electrons are heavier along the rotational axis but lighter along the perpendicular direction ($m_{\parallel} > m_{\perp}$). In this case, the introduced radial tension causes the upward movement of the conduction band ($+\Delta E$) along the orientation [100] and the downward movement of the conduction band ($-\Delta E$) along the orientation [001]. It should be noted that charge carriers tend to repopulate from the higher energy valley [100] to the lower energy valley [001]. In summary, the applied pressure causes the modulation of conduction bands and the mass shift of charge carriers, resulting in less electrons in the ellipsoid valley [100] whilst more electrons in the ellipsoid valley [001] in SiC close to the diaphragm center.

Fig. 6**b** presents the energy band diagram of 3C-SiC/Si heterojunction, the generation of electrons and holes under the light illumination, and the strain modulation on the conduction band and electron mass along the interested orientation [100]. When the heterojunction is excited by a suitable-wavelength laser, electron-hole pairs are generated, then separated to SiC and Si sides. As the electrodes are fabricated on SiC, only generated electrons affect the output photovoltage. Thus, the effect of applied strain on the effective mass and valence band of photogenerated holes in Si is ignored. As analyzed in Fig. 6**a**, the applied pressure creates less electrons in [100] energy valley and more electrons in the perpendicular valley. Since electron effective mass is heavier along the rotational axis, the induced tensile stress results in less heavy electrons ($m_{\parallel}$) but more light electrons ($m_{\perp}$) along the orientation [100]. Therefore, the average effective mass of photo-excited electrons is reduced, or the average electron mobility is increased under pressure.

Fig. 6**c, d** illustrates the concentration of photogenerated electrons in SiC under two cases of without and with applied pressure. Generated electrons in SiC diffuse evenly from the illumination spot under the no pressure condition. Under the applied pressure from the back side, the radial strain state changes continuously from tensile in the diaphragm center to compressive in the edge. As the reference electrode is arranged along the strain-insensitive orientation [110], the electron concentration under this electrode is almost constant. Along the strain-sensitive direction [100], the tensile strain increases the electron mobility in the area between the illumination spot and active electrode. Consequently, the smaller electron concentration under the active electrode means the smaller electron gradient between the active and reference electrodes when pressure is applied. This hypothesis is consistent with the decrease in the output voltage when increasing the applied pressure in all experiments. Considering the out-of-plane direction [001] from Si to SiC, the generation of electron-hole pairs under illumination and the energy band diagram of SiC/Si heterojunction under radial tensile strain are presented in Figure S4. Electron-hole pairs are created in Si only since the photon energy of 637-nm laser is less than the bandgap of 3C-SiC (1.95 eV $<$ 2.38 eV). The induced tensile strain causes the split of Si conduction band and the repopulation of light and heavy generated electrons. Therefore, there are more heavy electrons with lower potential energy or smaller barrier height ($\phi_{HE} < \phi_0$). Consequently, there are less electrons migrating from Si to SiC, which also contributes to the reduction in the photogenerated voltage under the applied pressure.

5. Conclusions

This paper investigates the piezo-optoelectronic coupling in heterojunctions for self-powered and ultrasensitive pressure sensing applications. A sensing device made of SiC/Si heterojunction is designed and fabricated to demonstrate the proof of the concept. The sensing chip features a circular SiC/Si diaphragm with active and reference electrodes along strain-sensitive [100] and strain-insensitive [110] orientations. The 637-nm laser with a power of 2.0 mW is kept illuminating at the diaphragm center, the photovoltage between two electrodes is recorded to monitor the applied pressure. Remarkably, the output voltage responses greatly to the change in both static and dynamic pressures. The larger pressure is applied, the lower output voltage is observed with a high resolution of 0.25% of the full scale. Gauge factor is found to be −670.2 which is much larger than the highest gauge factor of n-type 3C-SiC. The excellent performance is derived from the piezo-optoelectronic coupling in heterojunctions, which is detected by the electrodes along the strain-sensitive and strain-insensitive orientations. These results are remarkable toward the development of self-powered and ultrasensitive mechanical sensors. The piezo-optoelectronic coupling depends on various parameters, such as the doping concentration and thickness of SiC and Si, and the arrangement of electrodes on SiC. Studying the effect of these parameters for enhancing the strain sensitivity will be our future works.

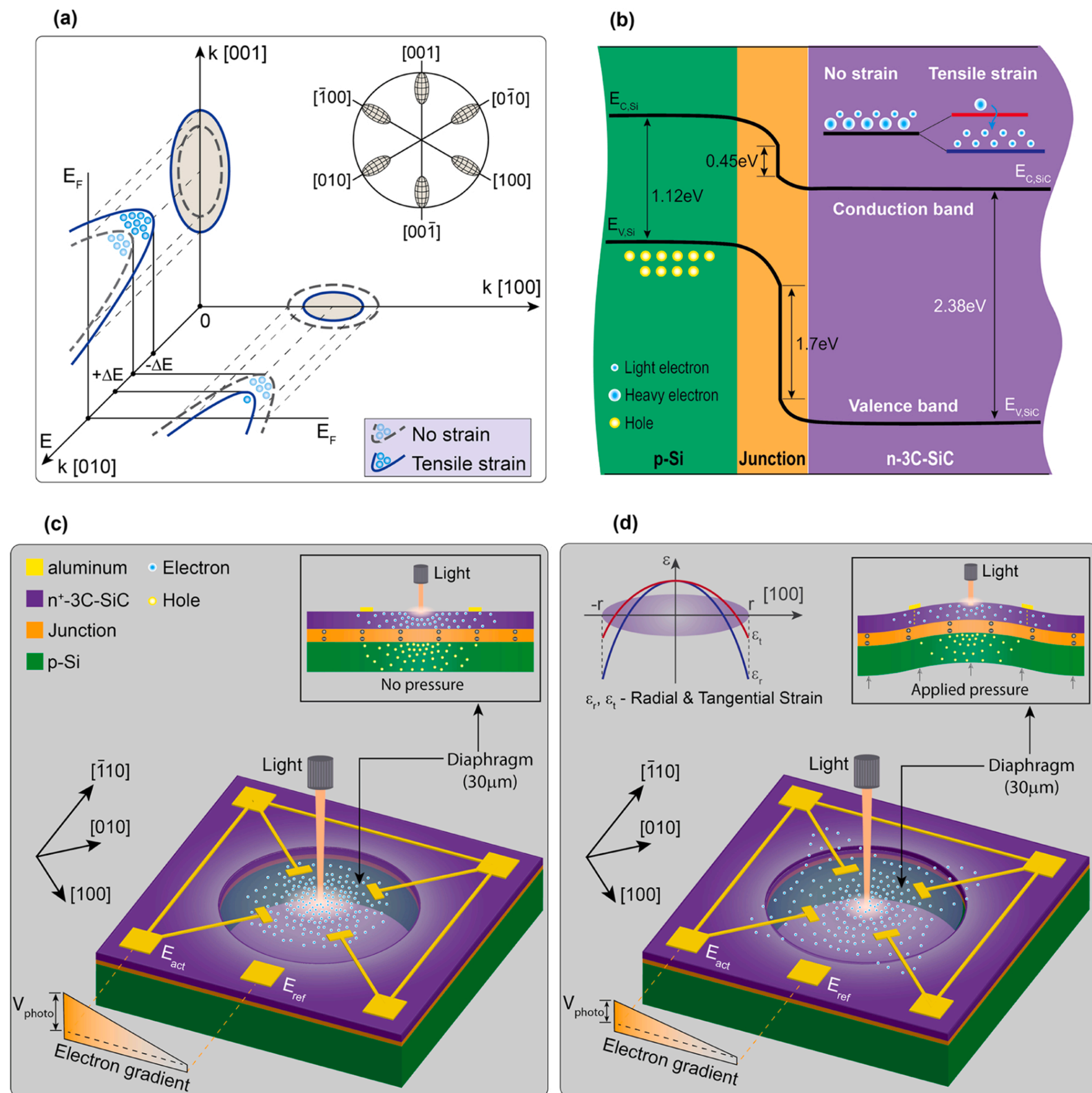

Fig. 6. Physical mechanism of the self-powered piezo-optoelectronic pressure sensor. (a) Conduction band split and mass shift of photogenerated electrons under radial tensile strain. (b) Energy band diagram of SiC/Si heterojunction along the orientation [100] under radial tensile strain. (c) Electron concentration under no pressure. (d) Electron concentration under applied pressure.

CRediT authorship contribution statement

Cong Thanh Nguyen: Writing – original draft, Investigation, Formal analysis, Data curation, Conceptualization. **Emily Lakis:** Investigation, Formal analysis, Conceptualization. **Dang D.H. Tran:** Investigation. **Tuan-Hung Nguyen:** Investigation. **Jun Sugawara:** Project administration, Funding acquisition, Conceptualization. **Ivan Gratchev:** Project administration, Funding acquisition, Conceptualization. **Erik W. Streed:** Writing – review & editing, Project administration, Funding acquisition. **Toan Dinh:** Writing – review & editing, Project administration, Funding acquisition. **Nam-Trung Nguyen:** Project administration, Funding acquisition. **Van Thanh Dau:** Writing – review & editing, Project administration, Investigation, Funding acquisition. **Dzung Viet Dao:** Writing – review & editing, Project administration, Investigation, Funding acquisition, Formal analysis, Conceptualization.

Declaration of Competing Interest

The authors declare that we have no known competing financial interests or personal relationships that could have appeared to influence the work reported in this paper.

Data availability

Data will be made available on request.

Acknowledgements

This work was supported by the Australian Research Council under Discovery Projects (DP220101252). This work used the Queensland node of the NCRIS-enabled Australian National Fabrication Facility (ANFF). The 3C-SiC/Si material was developed and supplied by the Queensland Micro and Nanotechnology Centre, part of the Queensland node-Griffith-of the Australian National Fabrication Facility, a company established under the National Collaborative Research Infrastructure Strategy to provide nano and microfabrication facilities for Australia's researchers. The sensing devices were also fabricated at the Queensland Micro and Nanotechnology Centre. The TEM and SAED images were

implemented by Centre for Microscopy and Microanalysis, The University of Queensland, Australia. The SEM image was taken at the Centre for Catalysis and Clean Energy, Griffith University by Mr. Duc Vu. Part of this paper is based on the research outcomes of the National Asset Centre of Excellence (NACOE) Project P139 Slopes – Development of wireless sensor network to predict rainfall-induced landslides. NACOE is a collaborative research agreement between the Queensland Department of Transport and Main Roads (TMR) and the Australian Road Research Board (ARRB). The authors are grateful for all supports of research centres and research funds.

Appendix A. Supporting information

Supplementary data associated with this article can be found in the online version at doi:10.1016/j.nanoen.2024.109477.

References

[1] Z.L. Wang, Toward self-powered sensor networks, Nano Today vol. 5 (6) (2010) 512–514.
[2] H. Zhang, Y. Yang, T.-C. Hou, Y. Su, C. Hu, Z.L. Wang, Triboelectric nanogenerator built inside clothes for self-powered glucose biosensors, Nano Energy vol. 2 (5) (2013) 1019–1024.
[3] C. Bai, et al., Wearable electronics based on the gel thermogalvanic electrolyte for self-powered human health monitoring, ACS Appl. Mater. Interfaces vol. 13 (31) (2021) 37316–37322.
[4] Z. Li, Q. Zheng, Z.L. Wang, Z. Li, Nanogenerator-based self-powered sensors for wearable and implantable electronics, Research (2020).
[5] T. Dinh, T. Nguyen, H.-P. Phan, N.-T. Nguyen, D.V. Dao, J. Bell, Stretchable respiration sensors: advanced designs and multifunctional platforms for wearable physiological monitoring, Biosens. Bioelectron. vol. 166 (2020) 112460.
[6] Z. Yu, et al., Bioinspired self-powered piezoresistive sensors for simultaneous monitoring of human health and outdoor UV light intensity, ACS Appl. Mater. Interfaces vol. 14 (4) (Feb 2 2022) 5101–5111, https://doi.org/10.1021/acsami.1c23604.
[7] C. Bowen, M. Arafa, Energy harvesting technologies for tire pressure monitoring systems, Adv. Energy Mater. vol. 5 (7) (2015) 1401787.
[8] Z.L. Wang, Triboelectric nanogenerator (TENG)—sparking an energy and sensor revolution, Adv. Energy Mater. vol. 10 (17) (2020) 2000137.
[9] T. Nguyen, T. Dinh, J. Bell, V.T. Dau, N.T. Nguyen, D.V. Dao, Light-harvesting self-powered monolithic-structure temperature sensing based on 3C-SiC/Si heterostructure, ACS Appl. Mater. Interfaces vol. 14 (19) (May 18 2022) 22593–22600, https://doi.org/10.1021/acsami.2c01681.
[10] C.T. Nguyen, K.T. Nguyen, T. Dinh, V.T. Dau, D.V. Dao, Wearable Physical Sensors for Non-invasive Health Monitoring. Wearable Biosensing in Medicine and Healthcare, Springer, 2024, pp. 111–132.
[11] M.A. Green, A. Ho-Baillie, H.J. Snaith, The emergence of perovskite solar cells, Nat. Photonics vol. 8 (7) (2014) 506–514.
[12] L. Huang, J. Chen, Z. Yu, D. Tang, Self-powered temperature sensor with seebeck effect transduction for photothermal-thermoelectric coupled immunoassay, Anal. Chem. vol. 92 (3) (Feb 4 2020) 2809–2814, https://doi.org/10.1021/acs.analchem.9b05218.
[13] C.T. Nguyen, et al., Photovoltaic effect-based multifunctional photodetection and position sensing using a 3C-SiC/Si heterojunction, ACS Appl. Electron. Mater. (2023), https://doi.org/10.1021/acsaelm.3c01145.
[14] Y. Kanda, Piezoresistance effect of silicon, Sens. Actuators A: Phys. vol. 28 (2) (1991) 83–91.
[15] L. Zhou, Q. Xin, J. Lin, S. Liang, G. Yang, A low-cost hydrogel with high conductivity and flexibility for pressure sensor and supercapacitor, Appl. Mater. Today vol. 34 (2023), https://doi.org/10.1016/j.apmt.2023.101907.
[16] T.-K. Nguyen, et al., Highly sensitive 4H-SiC pressure sensor at cryogenic and elevated temperatures, Mater. Des. vol. 156 (2018) 441–445, https://doi.org/10.1016/j.matdes.2018.07.014.
[17] L. Pan, et al., An ultra-sensitive resistive pressure sensor based on hollow-sphere microstructure induced elasticity in conducting polymer film, Nat. Commun. vol. 5 (2014) 3002, https://doi.org/10.1038/ncomms4002.
[18] C.S. Smith, Piezoresistance effect in germanium and silicon, Phys. Rev. vol. 94 (1) (1954) 42.
[19] J.S. Shor, D. Goldstein, A.D. Kurtz, Characterization of n-type beta-SiC as a piezoresistor, IEEE Trans. Electron Devices vol. 40 (6) (1993) 1093–1099.
[20] H.-P. Phan, et al., Piezoresistive effect of p-type single crystalline 3C-SiC thin film, IEEE Electron Device Lett. vol. 35 (3) (2014) 399–401, https://doi.org/10.1109/led.2014.2301673.
[21] Y. Kanda, A graphical representation of the piezoresistance coefficients in silicon, IEEE Trans. Electron Devices vol. 29 (1) (1982) 64–70.
[22] A. Qamar, T. Dinh, M. Jafari, A. Iacopi, S. Dimitrijev, D.V. Dao, A large pseudo-Hall effect in n-type 3C-SiC(1 0 0) and its dependence on crystallographic orientation for stress sensing applications, Mater. Lett. vol. 213 (2018) 11–14, https://doi.org/10.1016/j.matlet.2017.10.117.
[23] R.S. Okojie, A.A. Ned, A.D. Kurtz, W.N. Carr, Characterization of highly doped n- and p-type 6H-SiC piezoresistors, IEEE Trans. Electron Devices vol. 45 (4) (1998) 785–790.
[24] H.-P. Phan, et al., Thickness dependence of the piezoresistive effect in p-type single crystalline 3C-SiC nanothin films, J. Mater. Chem. C vol. 2 (35) (2014) 7176–7179, https://doi.org/10.1039/c4tc01054j.
[25] A. Lugstein, M. Steinmair, A. Steiger, H. Kosina, E. Bertagnolli, Anomalous piezoresistance effect in ultrastrained silicon nanowires, Nano Lett. vol. 10 (8) (Aug 11 2010) 3204–3208, https://doi.org/10.1021/nl102179c.
[26] R. He, P. Yang, Giant piezoresistance effect in silicon nanowires, Nat. Nanotechnol. vol. 1 (1) (Oct 2006) 42–46, https://doi.org/10.1038/nnano.2006.53.
[27] J. Milne, A. Rowe, S. Arscott, C. Renner, Giant piezoresistance effects in silicon nanowires and microwires, Phys. Rev. Lett. vol. 105 (22) (2010) 226802.
[28] A. Waseem, et al., Flexible self-powered piezoelectric pressure sensor based on GaN/p-GaN coaxial nanowires, J. Alloy. Compd. vol. 872 (2021), https://doi.org/10.1016/j.jallcom.2021.159661.
[29] G. Yao, et al., Bioinspired triboelectric nanogenerators as self-powered electronic skin for robotic tactile sensing, Adv. Funct. Mater. vol. 30 (6) (2019), https://doi.org/10.1002/adfm.201907312.
[30] H.-P. Phan, D.V. Dao, K. Nakamura, S. Dimitrijev, N.-T. Nguyen, The piezoresistive effect of SiC for MEMS sensors at high temperatures: a review, J. Micro Syst. vol. 24 (6) (2015) 1663–1677.
[31] T. Dinh, et al., Thermoresistance of p -Type 4H–SiC integrated MEMS devices for high-temperature sensing, Adv. Eng. Mater. vol. 21 (3) (2019), https://doi.org/10.1002/adem.201801049.
[32] X. She, A.Q. Huang, O. Lucia, B. Ozpineci, Review of silicon carbide power devices and their applications, IEEE Trans. Ind. Electron. vol. 64 (10) (2017) 8193–8205.
[33] T.-H. Nguyen, et al., Ultrasensitive self-powered position-sensitive detector based on n-3C-SiC/p-Si heterojunctions, ACS Appl. Electron. Mater. vol. 4 (2) (2022) 768–775, https://doi.org/10.1021/acsaelm.1c01156.
[34] D.V. Dao, Study on silicon piezoresistive six-degree of freedom micro force-moment sensors and application to fluid mechanics (Doctoral thesis), Ritsumeikan University, 2003.
[35] T.-K. Nguyen, et al., Experimental investigation of piezoresistive effect in p-type 4H–SiC, IEEE Electron Device Lett. vol. 38 (7) (2017) 955–958, https://doi.org/10.1109/led.2017.2700402.
[36] T.-H. Nguyen, et al., Giant lateral photovoltage in a SiC/Si heterojunction with a micro free-standing SiC serpentine beam, ACS Appl. Energy Mater. vol. 5 (8) (2022) 9830–9836, https://doi.org/10.1021/acsaem.2c01552.
[37] T. Nguyen, et al., The concept of light-harvesting, self-powered mechanical sensors using a monolithic structure, Nano Energy vol. 96 (2022), https://doi.org/10.1016/j.nanoen.2022.107030.
[38] C.T. Nguyen, et al., Vertical piezo-optoelectronic coupling in 3C-SiC/Si heterostructure for self-powered and highly-sensitive mechanical sensing, ACS Appl. Mater. Interfaces (2023) 28781–28789, https://doi.org/10.1021/acsami.3c03045.
[39] L. Wang, S. Dimitrijev, J. Han, P. Tanner, A. Iacopi, L. Hold, Demonstration of p-type 3C–SiC grown on 150 mm Si (1 0 0) substrates by atomic-layer epitaxy at 1000C, J. Cryst. Growth vol. 329 (1) (2011) 67–70.
[40] C.Q. Yu, H. Wang, Large near-infrared lateral photovoltaic effect observed in Co/Si metal-semiconductor structures, Appl. Phys. Lett. vol. 96 (17) (2010).
[41] B. Song, et al., Near-ultraviolet lateral photovoltaic effect in Fe 3 O 4/3C-SiC Schottky junctions, Opt. Express vol. 24 (21) (2016) 23755–23764.
[42] A.R. Md Foisal, et al., Self-powered broadband (UV-NIR) photodetector based on 3C-SiC/Si heterojunction, IEEE Trans. Electron Devices vol. 66 (4) (2019) 1804–1809, https://doi.org/10.1109/ted.2019.2899742.